Robotica: (2019) volume 37, pp. 1971–1986. © Cambridge University Press 2019
doi:10.1017/S0263574719000389

Kinetic and Dynamic Modeling of Single Actuator Wave-Like Robot

Ruoyu Feng, Peng Zhang, Junfeng Li and Hexi Baoyin*

School of Aerospace Engineering, Tsinghua University, Beijing 100084, China.
E-mails: fry18@mails.tsinghua.edu.cn, zhangpen18@mails.tsinghua.edu.cn, lijunf@mail.tsinghua.edu.cn

(Accepted March 3, 2019. First published online: April 10, 2019)

SUMMARY
In this study, the kinematics and dynamics of a single actuator wave (SAW)-like robot are explored. Comprising a helical spine and links, SAW has the potential for miniaturization. A kinematic model for SAW is firstly established, and the dynamic equation of motion is derived based on Kane's method. For validation, the motion of SAW is simulated using both MATLAB and ADAMS, and the comparison of results demonstrates the effectiveness of the theoretical models. Then the inverse dynamic analysis is performed to reveal the power consumption. Finally, robot prototypes are developed and tested to confirm the robot velocity predicted by simulations.

KEYWORDS: Wave-like robot; Single actuator; Modeling; Kane's method; Simulation.

Nomenclature

I($OXYZ$)	Inertial frame
U($oxyz$)	Moving reference frame attached to robot's head
L_i($o_i x_i y_i z_i$)	Link frame for link i
$\boldsymbol{e}_X/\boldsymbol{e}_Y/\boldsymbol{e}_Z$	Base vectors of frame I along X/Y/Z axis
A/k	Wave parameters representing the amplitude/ wave length
$\vartheta/\dot{\vartheta}$	Rotation angle/angular velocity of the motor
L_{wave}	Wave length
L_{link}	Length of each link (except for 0th links)
r	Half of the length of each link (except for 0th links)
m	Mass of each link (except for 0th links)
n	Number of links (except for 0th links)
L_0	Length of 0th links
C_i	Center of mass of each link
${}^{\text{U}}_{i}\boldsymbol{R}$	Transformation matrix from frame U to frame L_i:
${}^{j}\boldsymbol{P}_i/{}^{j}\boldsymbol{P}_{\text{tip}i}$	Coordinate of joint i/ link tip i in frame L_j
$\alpha_i/{}^{\text{U}}\boldsymbol{\Omega}_i/{}^{\text{U}}\dot{\boldsymbol{\Omega}}_i$	Inclination angle/angular velocity/angular acceleration of link i in frame U
${}^{\text{U}}\boldsymbol{P}_{Ci}/{}^{\text{U}}\boldsymbol{P}_{i+1}$	Coordinate of C_i/joint i with reference to frame U
${}^{\text{U}}\boldsymbol{V}_{Ci}/{}^{\text{U}}\dot{\boldsymbol{V}}_{Ci}$	Velocity/ acceleration of C_i in frame U
$\dot{x}_{\text{tip}i}$	Horizontal velocity of the link tip i in frame U
V_{lowest}	Horizontal velocity of the lowest tip in frame U
$F^{(r)}/F^{*(r)}$	rth generalized active/ generalized inertial force
u_r	rth generalized speed
$\boldsymbol{V}_k^{(r)}/\boldsymbol{\Omega}_k^{(r)}$	Partial velocities/partial angular velocities corresponding to u_r
V_{robot}	Velocity of the robot head in frame I
$\boldsymbol{V}_{\text{helix}}/\boldsymbol{V}_i$	Absolute velocity of the helix/ link i in frame I

* Corresponding author. E-mail: baoyin@tsinghua.edu.cn

https://doi.org/10.1017/S0263574719000389 Published online by Cambridge University Press

$\boldsymbol{\Omega}_{\text{helix}}/\boldsymbol{\Omega}_i$	Angular velocity of the helix/link i in frame I
T_{motor}	Motor torque
f_{head}/f_j	Sliding ground friction force acting on the robot head/link j
N_{head}/N_j	Ground reaction force acting on the robot head/link j
$\boldsymbol{F}^*_{\text{helix}}/\boldsymbol{F}^*_i$	Inertial force acting on the helix/link i
$\boldsymbol{M}^*_{\text{helix}}/\boldsymbol{M}^*_i$	Inertial moment acting on the helix/link i
M_{head}	Sum of the mass of the robot head and the helix
M_{robot}	Total mass of the robot
J_{helix}	Moment of inertia of the helix about X-axis
J_i	Moment of inertia of link i about Z-axis
$\mu_{\text{g}}/\mu_{\text{h}}$	Dynamic friction coefficient between links and ground/helix
$\bar{P}_{\text{motor}}$	Average mechanical output power of motor in one period
COT	Cost of transport defined to evaluate power consumption

1. Introduction

Bionic robots are in good performance with mechanical and electrical systems which imitate biological and motion characteristics of organisms according to the principles of bionics. The snake robots show a typical example because of their flexibility and environmental adaptivity. Two main locomotion patterns of snake robots have been investigated in the past years: the serpentine locomotion[1–3] and the traveling wave locomotion.[4–6] Compared with the former, the traveling wave locomotion provides snake robots with the ability to climb over obstacles and dive in the water. But traditional snake robots with these locomotions require redundant motors and complicated structure to realize motion, causing difficulties in motion control. Although several improvements in their actuation methods[7,8] and structures[9] have been considered, these snake robots still have a relatively large size. Zarrouk[10] recently presented a single actuator wave (SAW)-like robot with clever mechanical design. SAW is competent in many complex environments, like a snake robot with traveling wave locomotion. Compared with traditional snake robots, SAW has only one motor and can be miniaturized and applied to surgery or planet exploration tasks. This minimalistic concept can also inspire the design of other microrobots or undulating robots. A conceptual design for fish robots which has a similar mechanism with SAW was proposed by Gao.[11]

However, there has been no theoretical model depicting the dynamics of SAW. Accurate kinematic and dynamic analyses are essential for understanding the mechanisms and control of a robot, and in this study, we draw on the experience of snake robots researchers to present the mathematical models of SAW. There are several methods for dynamic modeling of snake robots. The conventional methods such as the Newton–Euler, method[12–14] and the Lagrange method[15,16] are not well suited for generating the dynamic equations of SAW in an explicit form. The recursive Newton–Euler formulation requires unnecessary calculations associated with the elimination of constraint forces of the joints between the links,[17] and the primary drawback of the Lagrange method for a multilink structure is the difficulty in deriving and differentiating the scalar Lagrangian function.

Kane's method uses generalized speeds rather than generalized coordinates, allowing one to focus on the motion aspects of robots rather than on their configurations.[18,19] In Kane's method, the constraint forces are masked under the generalized forces, and the interaction forces between the links and the helix are automatically eliminated.[20] It facilitates the generation of dynamical equations in an explicit, closed form,[21] especially in dealing with the multiplicity of masses in a system.[22] Kane's method has been applied to the dynamic analysis of snake robots with computational efficiency. For example, Nia[23] proposed a recursive algorithm of Kane's equation to model a snake robot, and Wei[24] solved the joint torques required to produce harmonic trapezoidal wave locomotion based on Kane's equations.

The dynamic analysis of SAW is complex because the constraint forces on links caused by the helix are unknown, a robot combining a mobile platform and a multilink structure also makes dynamic modeling more difficult. In these regards, Kane's method is employed to study this mechanism. In our theoretical model, some simplifications are made for the convenience of analysis such as neglecting the impacts between each robot parts during motion, since the lightweight parts will not cause intense impacts. A more accurate model can be developed in simulation software such as ADAMS to examine the effects of these simplifications.

https://doi.org/10.1017/S0263574719000389 Published online by Cambridge University Press

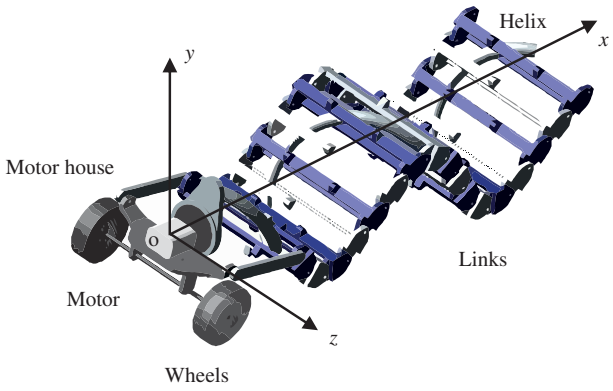


Fig. 1. The structure of SAW and the reference frame U(o*xyz*).

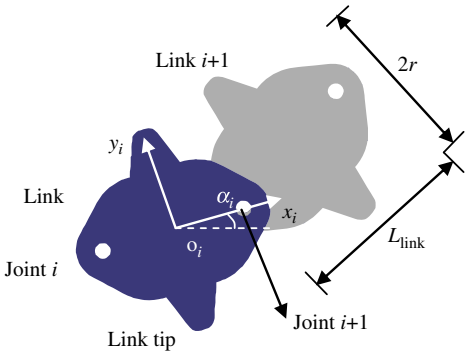


Fig. 2. The link frame $L_i(o_i x_i y_i z_i)$ on link i.

The objective of this study is to develop the kinematic and dynamic models for SAW. The paper starts by presenting these theoretical models of SAW. Comparisons of the robot velocities and motor torques obtained from the proposed theoretical model and ADAMS simulation are carried out. The influences of the friction and the robot length on the velocity and motion efficiency of SAW are evaluated. Finally, experiments conducted on robot prototypes are reported to validate the proposed model.

2. Kinematic Modeling

SAW is composed of four parts: the motor, the motor house with supportive wheels, the helix, and the series of links, as shown in Fig. 1. The helix is rotated by the motor, swinging the links to form an advancing sine wave. SAW moves in a horizontal plane, and its propelling force comes from the interaction of the link tips with the ground through friction.

Assuming that the robot consists of n links connected by $n-1$ revolute joints, the length L_{link}, height $2r$, and mass m are the same for each link. The mass of link i is uniformly distributed so that the link center of mass (CM), C_i ($i = 1,2, \ldots, n$), is located at its geometrical center.

SAW is modeled with respect to three right-handed reference frames, including the inertial frame I(*OXYZ*) and the moving orthonormal reference frame U(o*xyz*) which is attached to robot's head at the motor. The *X*- and *x*-axes are aligned with the axis of the helix, pointing toward the tail of SAW. The upward *Y*- and *y*-axes are vertical to the horizontal ground, as shown in Fig. 1. Two adjacent links i and $i+1$ are connected to each other by joint $i+1$. $L_i(o_i x_i y_i z_i)$ is denoted as the link frame for link i and originally coincide with C_i. The axis x_i is along the direction from joint i toward joint $i+1$, and the inclination angle of link i (between x and x_i) is α_i, as shown in Fig. 2. The position vector of C_i with reference to frame U is denoted by ${}^{\mathrm{U}}\boldsymbol{P}_{Ci} = [x_{Ci}, y_{Ci}, 0]^{\mathrm{T}}$.

2.1. Link position

In the frame U, the projection of the rotating helix onto the *xy* plane is an advancing sine wave. Assuming that all of the links are very short and are tangent to the wave at their CM, the following relationship holds:

https://doi.org/10.1017/S0263574719000389 Published online by Cambridge University Press

$$\tan\alpha_i = \left.\frac{\partial y}{\partial x}\right|_{x=x_{Ci}} = Ak\cos(kx_{Ci}+\vartheta) \tag{1}$$

C_i lies on the sinusoid, and its coordinates fulfill that

$$y_{Ci} = A\sin(kx_{Ci}+\vartheta) \tag{2}$$

where A is the wave amplitude, ϑ is the rotation angle of the motor. k represents the wave length L_{wave} and $k = 2\pi/L_{\text{wave}}$.

Denote the position vector of joint i with respective to the frame L_j as ${}^{j}\boldsymbol{P}_i$, that is, ${}^{i}\boldsymbol{P}_{i+1} = [L_{\text{link}}/2, 0, 0]^{\mathrm{T}}$. The position vector ${}^{\mathrm{U}}\boldsymbol{P}_{i+1}$ of joint $i+1$ in the frame U is obtained using a combination of the translation and rotation transformations as follows:

$${}^{\mathrm{U}}\boldsymbol{P}_{i+1} = {}^{\mathrm{U}}\boldsymbol{P}_{Ci} + {}^{\mathrm{U}}_{i}\boldsymbol{R}\,{}^{i}\boldsymbol{P}_{i+1} \tag{3a}$$

$${}^{\mathrm{U}}\boldsymbol{P}_{i+1} = {}^{\mathrm{U}}\boldsymbol{P}_{Ci+1} + {}^{\mathrm{U}}_{i+1}\boldsymbol{R}\,{}^{i+1}\boldsymbol{P}_{i+1} \tag{3b}$$

where ${}^{\mathrm{U}}_{i}\boldsymbol{R}$ is the transformation matrix from the frame U to the link frame L_i:

$${}^{\mathrm{U}}_{i}\boldsymbol{R} = \begin{bmatrix} \cos\alpha_i & -\sin\alpha_i & 0 \\ \sin\alpha_i & \cos\alpha_i & 0 \\ 0 & 0 & 1 \end{bmatrix} \tag{4}$$

From Eq. (3), the constraint equation of joint $i+1$ can be expressed as:

$${}^{\mathrm{U}}\boldsymbol{P}_{Ci} + {}^{\mathrm{U}}_{i}\boldsymbol{R}\,{}^{i}\boldsymbol{P}_{i+1} - {}^{\mathrm{U}}\boldsymbol{P}_{Ci+1} - {}^{\mathrm{U}}_{i+1}\boldsymbol{R}\,{}^{i+1}P_{i+1} = \boldsymbol{0} \tag{5}$$

The first term of Eq. (5) is

$$x_{Ci+1} - x_{Ci} - L_{\text{link}}\cdot(\cos\alpha_i + \cos\alpha_{i+1})/2 = 0 \tag{6}$$

The first two longer links of length L_0, which connect the motor house and other links and rotate about a fixed axis, are denoted by 0th links. According to the geometric relationship of 0th links, the coordinate of the first joint ${}^{\mathrm{U}}\boldsymbol{P}_1 = [x_1, y_1, 0]^{\mathrm{T}}$ satisfies:

$$\begin{cases} x_1^2 + y_1^2 = L_0^2 \\ \alpha_1 = \arctan\left(Ak\cdot\cos(kx_{C1}+\vartheta)\right) \\ x_1 = x_{C1} - (L_{\text{link}}\cdot\cos\alpha_1)/2 \\ y_1 = y_{C1} - (L_{\text{link}}\cdot\sin\alpha_1)/2 = A\sin(kx_{C1}+\vartheta) - (L_{\text{link}}\cdot\sin\alpha_1)/2 \end{cases} \tag{7}$$

Then x_{C1} can be solved and used as a starting term to determine the position of each moving link based on the recursion relation Eqs. (6) and (1). A numerical technique is required to solve these nonlinear implicit recursion formulas. It can be proved that y_{Ci} and y_{Ci+1} automatically satisfy Eq. (5) since L_{link} and the relative angle between two adjacent links, $\alpha_{i+1} - \alpha_i$, is very small.

2.2. Link velocity

(1) CM velocity and angular velocity of link

Taking the time derivative on Eq. (5), the constraint equation between the velocities of the adjacent link i and link $i+1$ is obtained:

$${}^{\mathrm{U}}\boldsymbol{V}_{Ci} + {}^{\mathrm{U}}\boldsymbol{\Omega}_i \times \left({}^{\mathrm{U}}_{i}\boldsymbol{R}\,{}^{i}\boldsymbol{P}_{i+1}\right) - {}^{\mathrm{U}}\boldsymbol{V}_{Ci+1} - {}^{\mathrm{U}}\boldsymbol{\Omega}_{i+1} \times \left({}^{\mathrm{U}}_{i+1}\boldsymbol{R}\,{}^{i+1}\boldsymbol{P}_{i+1}\right) = \boldsymbol{0} \tag{8}$$

where ${}^{\mathrm{U}}\boldsymbol{\Omega}_i = [0, 0, \dot{\alpha}_i]^{\mathrm{T}}$ and ${}^{\mathrm{U}}\boldsymbol{V}_{Ci} = [\dot{x}_{Ci}, \dot{y}_{Ci}, 0]^{\mathrm{T}}$ are the angular velocity of link i and the relative velocity of C_i in the frame U, respectively.

The first term in Eq. (8) is

$$\dot{x}_{Ci+1} - \dot{x}_{Ci} + L_{\text{link}}\frac{\dot{\alpha}_i\cdot\sin\alpha_i + \dot{\alpha}_{i+1}\cdot\sin\alpha_{i+1}}{2} = 0 \tag{9}$$

where α_i and α_{i+1} can be determined after the link positions are solved. The horizontal velocity of each link CM can be solved after the angular velocities $\dot{\alpha}_i$ and $\dot{x}_{C1}$ are obtained. From the "chain rule," the angular velocity of link i is the time derivative of α_i in Eq. (1),

https://doi.org/10.1017/S0263574719000389 Published online by Cambridge University Press

$$\dot{\alpha}_i = \frac{\partial \alpha_i}{\partial x_{Ci}} \dot{x}_{Ci} + \frac{\partial \alpha_i}{\partial \vartheta} \dot{\vartheta} = \beta_i \cdot (\dot{x}_{Ci} + \dot{\vartheta}/k) \tag{10}$$

where $\dot{\vartheta}$ is the motor rotation velocity, $\beta_i = -k^2 \cdot \cos^2 \alpha_i \cdot y_{Ci}$, and $\dot{\vartheta}/k$ is the wave speed of the traveling wave locomotion.

Substituting Eq. (10) into Eq. (9) gives the following velocity recursive equation:

$$\dot{x}_{Ci+1} = \dot{x}_{Ci} \cdot \frac{2 - L_{\text{link}} \cdot \beta_i \sin \alpha_i}{2 + L_{\text{link}} \cdot \beta_{i+1} \sin \alpha_{i+1}} - \frac{L_{\text{link}}(\beta_i \sin \alpha_i + \beta_{i+1} \sin \alpha_{i+1}) \cdot \dot{\vartheta}}{k(2 + L_{\text{link}} \cdot \beta_{i+1} \sin \alpha_{i+1})} \tag{11}$$

Taking the time derivative in Eq. (2), the vertical velocity of the CM of link i, $\dot{y}_{Ci}$, is also obtained:

$$\dot{y}_{Ci} = \tan \alpha_i \cdot (\dot{x}_{Ci} + \dot{\vartheta}/k) \tag{12}$$

The horizontal velocity of the CM of the first link, $\dot{x}_{C1}$, is obtained by differentiating Eq. (7) with respect to time:

$$\dot{x}_{C1} = -\frac{\xi \cdot \dot{\vartheta}}{k(x_1 + \xi)} \tag{13}$$

where $\xi = y_1 \tan \alpha_1 + \beta_1 L_{\text{link}} \cdot (x_1 \sin \alpha_1 - y_1 \cos \alpha_1)/2$, and x_1 and y_1 are the coordinates of the first joint in the frame U. Eq. (13) can also be derived under the circumstance that the velocity of the first joint should be vertical to the rotating 0th links, see Appendix A.

(2) Horizontal velocity of link tip at wave trough

When SAW moves, the lowest tip of link locating around the wave trough is in touch with the ground. Assuming that there is no slip between the tips and the ground, the forward velocity of SAW should be equal to the backward horizontal velocity of the tip contacting the ground in the reference frame U (in the direction along the positive x-axis).

Suppose the distance between the link tip and the CM is r. Then the coordinate of the link tip i in the reference frame L_i is ${}^{i}\boldsymbol{P}_{\text{tip}i} = [0, -r, 0]^{\text{T}}$. The coordinate of tip i in the frame U, ${}^{\text{U}}\boldsymbol{P}_{\text{tip}i} = [x_{\text{tip}i}, y_{\text{tip}i}, 0]^{\text{T}}$, is given by:

$${}^{\text{U}}\boldsymbol{P}_{\text{tip}i} = {}^{\text{U}}\boldsymbol{P}_{Ci} + {}^{\text{U}}_{i}\boldsymbol{R}^{i}\boldsymbol{P}_{\text{tip}i} \tag{14}$$

After taking the derivative of $x_{\text{tip}i}$ in Eq. (14), the horizontal velocity of the link tip $\dot{x}_{\text{tip}i}$ is obtained:

$$\dot{x}_{\text{tip}i} = \dot{x}_{Ci} - rAk^2 \cdot \sin(kx_{Ci} + \vartheta) \cos^3 \alpha_i \cdot (\dot{\vartheta}/k + \dot{x}_{Ci}) \tag{15}$$

When the link i is near the wave trough, $\sin(kx_{Ci} + \vartheta) \approx -1$, $\alpha_i \approx 0$, Eq. (15) reduces to:

$$\dot{x}_{\text{tip}i} \approx \dot{x}_{\text{Ci}} \cdot \left(1 + rAk^2\right) + rAk \cdot \dot{\vartheta} \tag{16}$$

Note that $rAk \cdot \dot{\vartheta} = 2\pi \cdot rA\dot{\vartheta}/L_{\text{wave}}$, Eq. (16) indicates that the velocity of SAW can be improved by increasing the link height r, the motor rotation velocity $\dot{\vartheta}$, and the helix (wave) parameter A/L_{wave}.

2.3. Link acceleration

By differentiating Eqs. (10) and (12) with respect to time, the angular acceleration, $\ddot{\alpha}_i$, and the vertical acceleration, $\ddot{y}_{Ci}$, of the link i can be written as:

$$\ddot{\alpha}_i = \frac{\beta_i}{k}(k\ddot{x}_{Ci} + \ddot{\vartheta}) + \left(\beta_i y_{Ci} - \frac{1}{2}\right) \cdot \sin 2\alpha_i \cdot (k\dot{x}_{Ci} + \dot{\vartheta})^2 \tag{17}$$

$$\ddot{y}_{Ci} = \frac{\tan \alpha_i}{k}(k\ddot{x}_{Ci} + \ddot{\vartheta}) - y_{Ci}(k\dot{x}_{Ci} + \dot{\vartheta})^2 \tag{18}$$

The time derivative of Eq. (8) results in the following acceleration constraint equation of joint i+1:

$$\begin{aligned} &{}^{\text{U}}\dot{\boldsymbol{V}}_{Ci} + {}^{\text{U}}\dot{\boldsymbol{\Omega}}_i \times \left({}^{\text{U}}_{i}\boldsymbol{R}^{i}\boldsymbol{P}_{i+1}\right) + {}^{\text{U}}\boldsymbol{\Omega}_i \times \left({}^{\text{U}}\boldsymbol{\Omega}_i \times {}^{\text{U}}_{i}\boldsymbol{R}^{i}\boldsymbol{P}_{i+1}\right) - \\ &{}^{\text{U}}\dot{\boldsymbol{V}}_{Ci+1} - {}^{\text{U}}\dot{\boldsymbol{\Omega}}_{i+1} \times \left({}^{\text{U}}_{i+1}\boldsymbol{R}^{i+1}\boldsymbol{P}_{i+1}\right) - {}^{\text{U}}\boldsymbol{\Omega}_{i+1} \times \left({}^{\text{U}}\boldsymbol{\Omega}_{i+1} \times {}^{\text{U}}_{i+1}\boldsymbol{R}^{i+1}\boldsymbol{P}_{i+1}\right) = \boldsymbol{0} \end{aligned} \tag{19}$$

https://doi.org/10.1017/S0263574719000389 Published online by Cambridge University Press

where ${}^{\mathrm{U}}\dot{\boldsymbol{V}}_{Ci} = [\ddot{x}_{Ci}, \ddot{y}_{Ci}, 0]^{\mathrm{T}}$ and ${}^{\mathrm{U}}\dot{\boldsymbol{\Omega}}_i = [0, 0, \ddot{\alpha}_i]^{\mathrm{T}}$ are the CM acceleration and the angular acceleration of link i, respectively.

Substituting Eq. (17) into Eq. (19) yields the recursive equation for acceleration:

$$\ddot{x}_{Ci+1} = f_1(x_{Ci}, x_{Ci+1}, \vartheta) \cdot \ddot{x}_{Ci} + f_2\left(x_{Ci}, x_{Ci+1}, \vartheta, \dot{x}_{Ci}, \dot{x}_{Ci+1}, \dot{\vartheta}, \ddot{\vartheta}\right) \tag{20}$$

where

$$\begin{aligned} f_1 &= (2 - L_{\mathrm{link}} \cdot \beta_i \sin\alpha_i)/(2 + L_{\mathrm{link}} \cdot \beta_{i+1} \sin\alpha_{i+1}) \\ f_2 &= \frac{-L_{\mathrm{link}}}{2 + L_{\mathrm{link}} \cdot \beta_{i+1} \sin\alpha_{i+1}}(\gamma_i + \gamma_{i+1}) \\ \gamma_i &= \frac{\beta_i \sin\alpha_i}{k}\ddot{\vartheta} + \cos\alpha_i \cdot \dot{\alpha}_i^2 + \left(\beta_i y_{Ci} - \frac{1}{2}\right) \cdot \sin\alpha_i \sin 2\alpha_i \cdot (k\dot{x}_{Ci} + \dot{\vartheta})^2 \end{aligned} \tag{21}$$

The starting term $\ddot{x}_{C1}$ can be obtained by differentiating Eq. (13) with respect to time.

Now we have obtained three recursive formulas, which can be used to determine the position, velocity, and acceleration of each link in the frame U at each moment.

3. Dynamic Modeling

In this section, Kane's method is employed to perform the dynamic analysis of SAW's mechanism. For a system with f degrees of freedom, Kane's equation can be expressed as:

$$F^{(r)} + F^{*(r)} = 0 \ \ (r = 1, 2, \ldots, f) \tag{22}$$

where $F^{(r)}$ and $F^{*(r)}$ represent the rth generalized active force and generalized inertial force, respectively. $F^{(r)}$ and $F^{*(r)}$ can be determined by

$$F^{(r)} = \sum_{k=1}^{b} \boldsymbol{V}_k^{(r)} \cdot \boldsymbol{F}_k + \sum_{k=1}^{b} \boldsymbol{\Omega}_k^{(r)} \cdot \boldsymbol{M}_k = \sum_{k=1}^{b} \frac{\partial \boldsymbol{V}_k}{\partial u_r} \cdot \boldsymbol{F}_k + \sum_{k=1}^{b} \frac{\partial \boldsymbol{\Omega}_k}{\partial u_r} \cdot \boldsymbol{M}_k \tag{23a}$$

$$F^{*(r)} = \sum_{k=1}^{b} \boldsymbol{V}_k^{(r)} \cdot \boldsymbol{F}_k^{*} + \sum_{k=1}^{b} \boldsymbol{\Omega}_k^{(r)} \cdot \boldsymbol{M}_k^{*} = \sum_{k=1}^{b} \frac{\partial \boldsymbol{V}_k}{\partial u_r} \cdot \boldsymbol{F}_k^{*} + \sum_{k=1}^{b} \frac{\partial \boldsymbol{\Omega}_k}{\partial u_r} \cdot \boldsymbol{M}_k^{*} \tag{23b}$$

where b is the number of bodies in the system, $\boldsymbol{V}_k$ is the absolute CM velocity of the kth body, $\boldsymbol{\Omega}_k$ is the angular velocity of the kth body, $\boldsymbol{F}_k$ and $\boldsymbol{M}_k$ are the active force and moment on the kth body, $\boldsymbol{F}_k^*$ and $\boldsymbol{M}_k^*$ are the inertial force and moment, u_r is the rth generalized speed, $\boldsymbol{V}_k^{(r)}$ and $\boldsymbol{\Omega}_k^{(r)}$ are defined as the partial velocities and partial angular velocities corresponding to u_r, respectively. The absolute velocities are linear combinations of partial velocities with the generalized speeds as coefficients, and Kane's method can be interpreted as equilibrium of forces on the directions of partial velocities through the projection (dot product) in Eq. (23).

For SAW, the following $n + 2$ generalized speeds are chosen:

$$\begin{cases} u_i = \dot{x}_{Ci} \ (i = 1, 2, \ldots n) \\ u_{n+1} = \dot{\vartheta} \\ u_{n+2} = V_{\mathrm{robot}} \approx -\dot{x}_{\mathrm{tip}j} \end{cases} \tag{24}$$

where V_{robot} is the robot head velocity with respect to the inertial frame I, and $\dot{x}_{\mathrm{tip}j}$ is the horizontal velocity of the tip j which is contacting the ground at a wave trough in the frame U. Note that Kane's method has to be applied in the inertial frame I. While the velocities as well as the accelerations obtained from Section 2 are expressed in the frame U, when calculating $\boldsymbol{V}_k$ or $\boldsymbol{F}_k^*$ for SAW it is necessary to take the motion of frame U into consideration, by simply adding u_{n+2} or $\dot{u}_{n+2}$.

Let $\boldsymbol{e}_{\mathrm{X}}, \boldsymbol{e}_{\mathrm{Y}}, \boldsymbol{e}_{\mathrm{Z}}$ be the base vectors of the frame I, respectively. The absolute velocity and angular velocity of the helix, $\boldsymbol{V}_{\mathrm{helix}}$ and $\boldsymbol{\Omega}_{\mathrm{helix}}$, can be expressed in terms of generalized speeds as follows:

$$\begin{cases} \boldsymbol{V}_{\mathrm{helix}} = u_{n+2}\boldsymbol{e}_{\mathrm{X}} \\ \boldsymbol{\Omega}_{\mathrm{helix}} = u_{n+1}\boldsymbol{e}_{\mathrm{X}} \end{cases} \tag{25}$$

https://doi.org/10.1017/S0263574719000389 Published online by Cambridge University Press

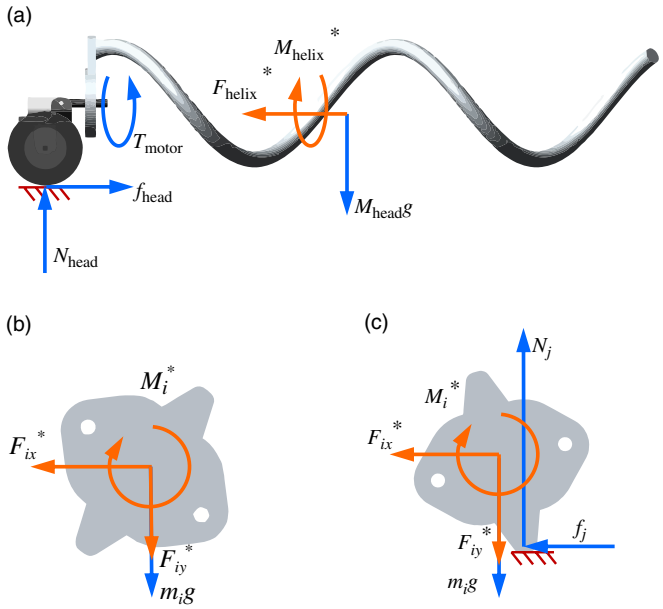


Fig. 3. Forces and moments on each part of SAW. (a) The forces and moments on the head and the helix. (b) On a link not contacting the ground. (c) On a link contacting the ground.

The absolute velocity $\boldsymbol{V}_i$ and the angular velocity $\boldsymbol{\Omega}_i$ of link i in the frame I are:

$$\boldsymbol{V}_i = (\dot{x}_{Ci} + V_{\text{robot}})\boldsymbol{e}_{\text{X}} + \dot{y}_{Ci}\boldsymbol{e}_{\text{Y}} \tag{26a}$$

$$\boldsymbol{\Omega}_i = \dot{\alpha}_i \boldsymbol{e}_{\text{Z}} \tag{26b}$$

Substituting the relative velocities (Eqs. (10) and (12)) into Eq. (26) gives

$$\begin{cases} \boldsymbol{V}_i = (u_i + u_{n+2})\boldsymbol{e}_{\text{X}} + \dfrac{\tan\alpha_i}{k}(ku_i + u_{n+1})\boldsymbol{e}_{\text{Y}} \\ \boldsymbol{\Omega}_i = \dfrac{\beta_i}{k}(ku_i + u_{n+1})\boldsymbol{e}_{\text{Z}} \end{cases} \tag{27}$$

Under no slipping condition, only u_{n+1} is independent variable among all generalized speeds. Besides, it can be proved that $u_i (i = 1, 2, \ldots n)$ and u_{n+2} are proportional to u_{n+1}.

The partial velocities and partial angular velocities corresponding to u_{n+1} are obtained from Eqs. (25) and (27), and are given by

$$\begin{cases} \boldsymbol{V}_{\text{helix}}^{(n+1)} = \frac{u_{n+2}}{u_{n+1}}\boldsymbol{e}_{\text{X}} \\ \boldsymbol{\Omega}_{\text{helix}}^{(n+1)} = \boldsymbol{e}_{\text{X}} \\ \boldsymbol{V}_i^{(n+1)} = \left(\dfrac{u_i}{u_{n+1}} + \dfrac{u_{n+2}}{u_{n+1}}\right)\boldsymbol{e}_{\text{X}} + \dfrac{\tan\alpha_i}{k}\left(k\dfrac{u_i}{u_{n+1}} + 1\right)\boldsymbol{e}_{\text{Y}} \\ \boldsymbol{\Omega}_i^{(n+1)} = \dfrac{\beta_i}{k}\left(k\dfrac{u_i}{u_{n+1}} + 1\right)\boldsymbol{e}_{\text{Z}} \end{cases} \tag{28}$$

The forces and torques acting on the helix and links are visualized in Fig. 3, where M_{head} is the sum of the mass of the robot head and the helix, and g is the gravitational acceleration. Considering the head and the helix as one part, the active forces include the gravitational forces $M_{\text{head}}g$, the sliding ground friction force acting on the wheel f_{head}, and the reaction force N_{head}. The active moments include the motor torque T_{motor} and the moment of f_{head} and N_{head} about CM of this part.

For a link off the ground, the active force is only the gravitational force m_ig. For the link j contacting with the ground, the active forces include the same m_ig, the ground friction force acting on the link tip, f_j, and the reaction force N_j. The contacting link is located at the wave trough, with α_j being very small and its tip being the lowest tip approximately.

https://doi.org/10.1017/S0263574719000389 Published online by Cambridge University Press

The active forces acting on each part and the active moments about the CM of each part are summarized as:

$$\begin{cases} \boldsymbol{F}_{\text{helix}} = f_{\text{head}}\boldsymbol{e}_{\text{X}} + \left(N_{\text{head}} - M_{\text{head}}g\right)\boldsymbol{e}_{\text{Y}} \\ \boldsymbol{M}_{\text{helix}} = T_{\text{motor}}\boldsymbol{e}_{\text{X}} + \left(f_{\text{head}} \cdot y_{\text{Chelix}} - N_{\text{head}} \cdot x_{\text{Chelix}}\right)\boldsymbol{e}_{\text{Z}} \\ \boldsymbol{F}_{i,\text{NC}} = -m_i g\boldsymbol{e}_{\text{Y}} \\ \boldsymbol{M}_{i,\text{NC}} = \boldsymbol{0} \\ \boldsymbol{F}_{j,\text{C}} = -f_j\boldsymbol{e}_X + \left(N_j - m_i g\right)\boldsymbol{e}_{\text{Y}} \\ \boldsymbol{M}_{j,\text{C}} \approx \left(N_j \cdot r \cdot \alpha_j - f_j \cdot r\right)\boldsymbol{e}_{\text{Z}} \end{cases} \tag{29}$$

where x_{Chelix} and y_{Chelix} are the coordinates of the head-helix CM, letter NC stands for "not contacting", and letter C stands for "contacting."

The CM acceleration $\boldsymbol{A}_i$ and angular acceleration $\dot{\boldsymbol{\Omega}}_i$ of link i with respective to the reference frame I can be calculated by Eqs. (17) and (18), respectively, and adding the robot head acceleration $\dot{u}_{n+2}$

$$\begin{aligned} \boldsymbol{A}_i &= (\dot{u}_i + \dot{u}_{n+2})\boldsymbol{e}_X + \left[\frac{\tan\alpha_i}{k}(k\dot{u}_i + \dot{u}_{n+1}) - y_{Ci}(ku_i + u_{n+1})^2\right]\boldsymbol{e}_Y \\ \dot{\boldsymbol{\Omega}}_i &= \left[\frac{\beta_i}{k}(k\dot{u}_i + \dot{u}_{n+1}) + \left(\beta_i y_{ci} - \tfrac{1}{2}\right) \cdot \sin 2\alpha_i \cdot (ku_i + u_{n+1})^2\right]\boldsymbol{e}_Z \end{aligned} \tag{30}$$

The inertial forces and moments acting on the helix and links are:

$$\begin{cases} \boldsymbol{F}^*_{\text{helix}} = -M_{\text{head}}\dot{u}_{n+2}\boldsymbol{e}_X \\ \boldsymbol{M}^*_{\text{helix}} = -J_{\text{helix}}\dot{u}_{n+1}\boldsymbol{e}_X \\ \boldsymbol{F}^*_i = -m_i\boldsymbol{A}_i \\ \boldsymbol{M}^*_i = -J_i\dot{\boldsymbol{\Omega}}_i \end{cases} \tag{31}$$

where J_{helix} and J_i are the moment of inertia of the helix about X-axis and the moment of inertia of link i about Z-axis, respectively.

Substituting the above terms into Kane's equation (Eq. (22)) results in the equation of motion:

$$\begin{aligned} T_{\text{motor}} \cdot \dot{\vartheta} &= -f_{\text{head}} \cdot V_{\text{robot}} + m_i g \sum_{i=1}^{n}\left[(\dot{x}_{Ci} + \dot{\vartheta}/k)\tan\alpha_i\right] \\ &\quad + \left(1 + rAk^2\right)\sum_{j}^{\text{C}}(\dot{x}_{Cj}f_j) + (V_{\text{robot}} + rAk\dot{\vartheta})\sum_{j}^{\text{C}}f_j \\ &\quad - \left(1 + rAk^2\right)\sum_{j}^{\text{C}}(\dot{x}_{Cj} + \dot{\vartheta}/k) \cdot N_j\alpha_j + M_{\text{head}}V_{\text{robot}}\dot{V}_{\text{robot}} + J_{\text{helix}}\dot{\vartheta}\ddot{\vartheta} \\ &\quad + \sum_{i=1}^{n}\left\{\begin{array}{l} m_i(\dot{x}_{Cj} + V_{\text{robot}})(\ddot{x}_{Cj} + \dot{V}_{\text{robot}}) \\ + \left(m_i\tan^2\alpha_i + J_i/\beta_i^2\right)(\dot{x}_{Ci} + \dot{\vartheta}/k)(\ddot{x}_{Ci} + \ddot{\vartheta}/k) \\ + k^2\left[J_i\beta_i\left(\beta_i y_{ci} - \tfrac{1}{2}\right) \cdot \sin 2\alpha_i - m_i y_{ci}\tan\alpha_i\right]\left(\dot{x}_{Ci} + \dot{\vartheta}/k\right)^3 \end{array}\right\} \end{aligned} \tag{32}$$

There are $n+2$ generalized speeds, so $n+1$ velocity constraints on SAW are required to combine Eq. (32) to perform dynamic analysis. Under no slipping condition, the following relation holds:

$$V_{\text{robot}} \approx -\dot{x}_{\text{tip}j} = -\left(1 + rAk^2\right)\dot{x}_{Cj} - rAk\dot{\vartheta} \tag{33}$$

The constraint provided by joint 1 on $\dot{x}_{C1}$ is Eq. (13), and the constraint provided by other n-1 joints is Eq. (11)). $n+2$ equations are given in Eqs. (11), (13), (32), and (33), which can be solved for the $n+2$ unknown variables. Substituting Eq. (33) into Eq. (32), the friction force terms with f_j can be eliminated, which implies that the ground friction does not contribute to the motor power dissipation (the term $\dot{\vartheta} \cdot T_{\text{motor}}$ in Eq. (32)) under no slipping condition, resulting in a highly efficient motion.

https://doi.org/10.1017/S0263574719000389 Published online by Cambridge University Press

Table I. Simulation parameters.

Size parameters							
Cycles of the helix (wave number)	Wave length L_{wave}/cm	Wave amplitude A/cm	Helix axis diameter /cm	Link length L_{link}/cm	Link height r/cm	Number of links n	0th link length L_0/cm
2	10.6	2.1	0.6	1.4	1.0	17	4.2
Contact parameters between ground and links							
Contact stiffness /N · cm^{-1}	Force exponent	Damping /N · s · cm^{-1}	Penetration depth/cm	Static friction coefficient	Dynamic friction coefficient μ_g	Static transition velocity /cm · s^{-1}	Dynamic transition velocity /cm · s^{-1}
11,500	2	6.8	0.01	$\mu_g + 0.05$	0.1∼1.5	0.01	1
Contact parameters between helix and links							
Contact stiffness /N · cm^{-1}	Force exponent	Damping /N · s · cm^{-1}	Penetration depth/cm	Static friction coefficient	Dynamic friction coefficient μ_h	Static transition velocity /cm · s^{-1}	Dynamic transition velocity /cm · s^{-1}
11,500	2	6.8	0.01	$\mu_h + 0.05$	0.1∼0.4	0.01	1
Inertial parameters							
Link mass m_i/g	link moment of inertia J_i/g · cm^2	Helix moment of inertia J_{helix}/g · cm^2	Helix mass M_{helix}/g	M_{head}/g	Total mass M_{robot}/g		
3.52	1.04	65.17	16.43	81.1	140.94		

A correction term can be introduced for other factors such as impacts, according to professional simulation software or experiments.

4. Simulation Study

4.1. Simulation parameters

To validate the proposed theoretical model of the SAW and to further study the motion of the robot, simulations are performed by MATLAB and the software ADAMS. The ADAMS model is shown in Fig. 1. The acceleration of gravity is $g = 9.8067\ \text{m} \cdot \text{s}^{-2}$, and other necessary parameters for the simulation are given in Table I. The motor rotation velocity is $\dot{\vartheta} = 2\pi$ rad/s. The simulation time is set to 5 s, and 500 time steps per period ($T = 1$ s) are used.

In ADAMS model, all parts are designed in CAD software and assembled in ADAMS to ensure accuracy. The motor axis is aligned with the helix axis. Links are connected by revolute joints which only have one rotational degree of freedom. The helix and the motor axis are connected by a motor-actuated revolute joint. The gap width between the helix and each link is 2 mm, where impact contacts would happen. In order to realize motion, a long runway under the model is created as well as the corresponding contacts. The normal and frictional contact forces are calculated using the inbuilt impact function algorithm in ADAMS, with the parameters listed in Table I. The inertial parameters set in MATLAB are directly calculated by ADAMS.

4.2. Kinematic simulations

The robot head is fixed at first to show the wave-like locomotion in the frame U. Figure 4 shows the trajectories of the link CMs and the link tips in five complete cycles from ADAMS, which are very close to that obtained by MATLAB; see Fig. 5. Figure 5 also marks the trajectories of the link tips

https://doi.org/10.1017/S0263574719000389 Published online by Cambridge University Press

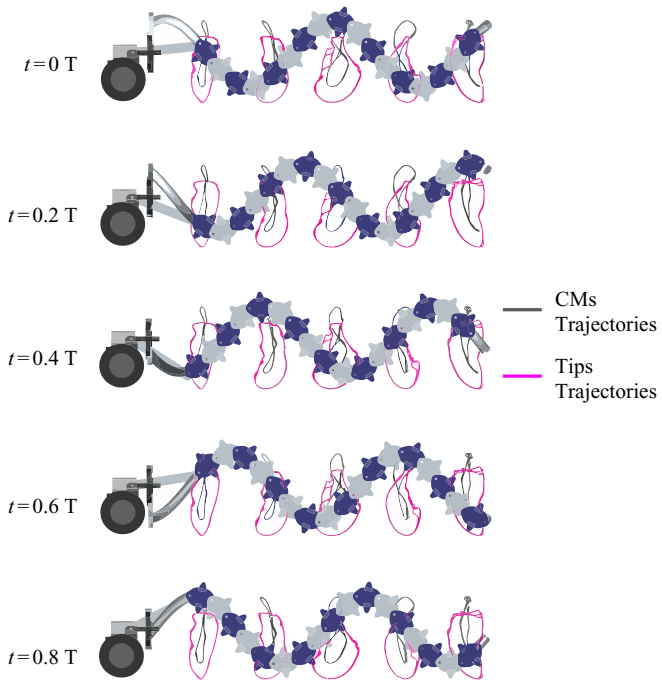


Fig. 4. Trajectories of the links obtained by ADAMS.

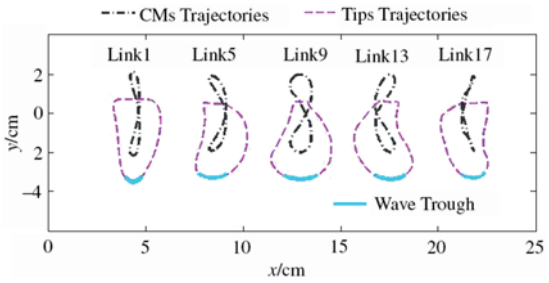


Fig. 5. Trajectories of the links obtained by MATLAB.

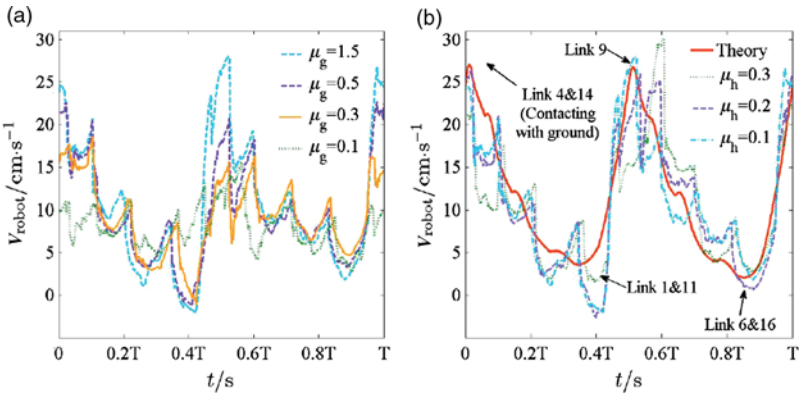


Fig. 6. Velocity of SAW. (a)Velocity vs. ground friction ($\mu_h = 0.1$). (b)Velocity vs. helix friction ($\mu_g = 1.5$).

when they are at the wave trough and contacting with the ground. The shapes of these trajectories are not uniform, indicating that the motion of one link would squeeze its neighboring links through joints.

After reliving the fixed constraint on the robot head and creating a runway, SAW will progress forward. The influence of the ground friction and the helix friction on the robot head velocity V_{robot} during one period is presented in Fig. 6(a) and (b), respectively. The increase of the ground friction

https://doi.org/10.1017/S0263574719000389 Published online by Cambridge University Press

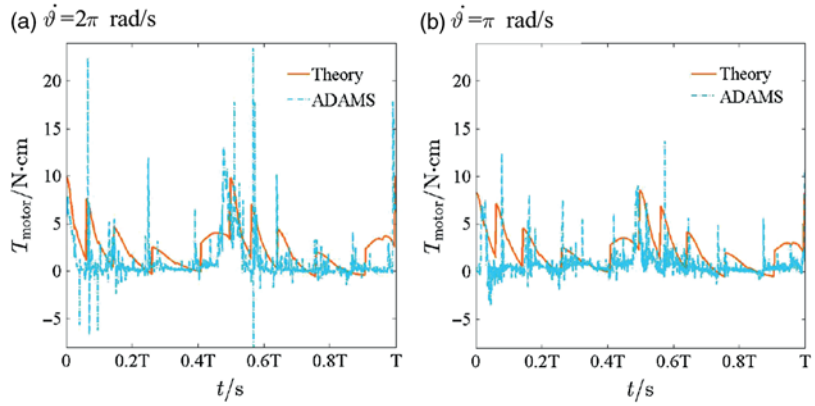


Fig. 7. Motor torque comparison of the theoretical model and the ADAMS model. (a)$\dot{\vartheta} = 2\pi$ rad/s. (b) $\dot{\vartheta} = \pi$ rad/s.

results in larger average velocity and produces a more intense velocity fluctuation over the time interval. Parts of the four curves coincide, which implies that some links slip while the other links still move without slipping when the ground friction is low. By keeping a constant $\mu_g = 1.5$, the V_{robot} for different μ_h are compared in Fig. 6(b). It turns out that within this range μ_h has little influence on the robot velocity. Rather than the helix friction, it is the normal constraint forces which drive the links to form a traveling wave.

In the MATLAB simulation, the horizontal velocity of the lowest tip in frame U, V_{lowest} is adopted to predict the robot head velocity under no slipping condition. Though SAW may have more than one tip contacting the ground, the motions of different tips at different wave troughs show only slight differences in calculation results, like a parallel four-bar linkage mechanism. The difference between the robot velocities obtained from ADAMS and MATLAB is shown in Fig. 6(b) for $\mu_g = 1.5$, which is large enough to ensure no slipping. When $\mu_h = 0.1$, the relative difference between the average velocity obtained by ADAMS $\bar{V}_{robot} = 10.41$ cm/s and the theoretical value $\bar{V}_{lowest} = 11.21$ cm/s is 7.14%. The maximum velocity predicted by ADAMS is 28.04 cm/s, which is also close to the theoretical value 27.49 cm/s. These demonstrate that V_{lowest} can approximate the velocity of SAW.

In this model, every 10 links form a complete period of the wave. These 10 links would contact with the ground at different duration of time, as marked in Fig. 6(b), making the motion of SAW analogous to a multi-legged robot with different stride length of links (see Fig. 5). As a result V_{robot} fluctuates though the motor rotates at a constant rate. It is also found from the simulation results that when the number of links is changed, the robot velocity has no obvious difference as long as SAW could form at least one complete wave cycle (10 links), see Fig. 8(c).

4.3. Inverse dynamics

The inverse dynamics analysis is performed to obtain the required motor torque. A comparison of the theoretical values of motor torque predicted by Eq. (32) using MATLAB and the results obtained from ADAMS when $\mu_g = 1.5$ and $\mu_h = 0.1$ is shown in Fig. 6. While both curves show similar trends, the ADAMS curves oscillate more intensely and have larger amplitude triggered by the impacts considered in the ADAMS model. The decrease of the actuation speed results in the mitigation of impacts. As a result, the motor torque obtained from ADAMS is closer to the theoretical model, as shown in Fig. 7(b). The theoretical curves also contain 10 sharp peaks, because the inclination angle α_j of the link touching the ground is not continuous when the 10 links in one cycle of wave successively touch the ground. In the theoretical model, being located at the lowest position is used as a criterion to judge the link contacting the ground, so the contact time is different from the ADAMS model. Besides, the maximum required torque is less than the stall torque of an ordinary DC geared motor. Since the peak torques in a short time would have no noticeable influence on total power consumption, we can conclude that the drive method for this type of robot is feasible.

The cost of transport, COT, is defined to evaluate the power consumption of motion as follows:

$$\mathrm{COT} = \frac{\bar{P}_{motor}}{M_{robot} g \cdot \bar{V}_{robot}} \tag{34}$$

https://doi.org/10.1017/S0263574719000389 Published online by Cambridge University Press

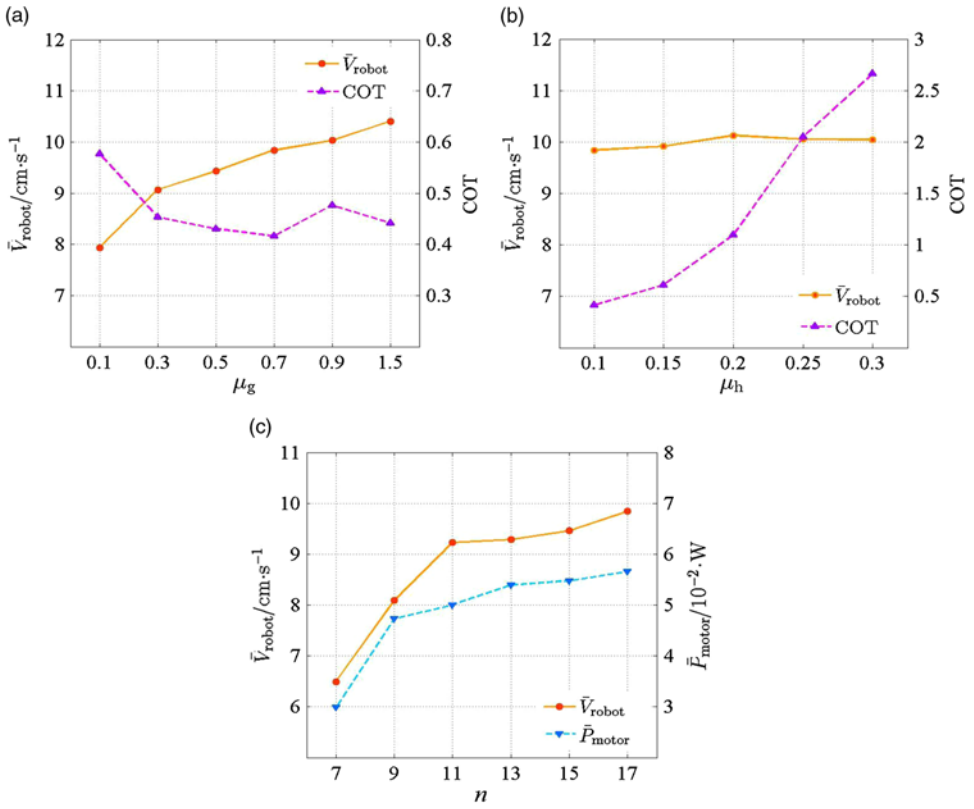


Fig. 8. Effect of frictions and link number on the motion of SAW. (a) Effect of ground friction ($\mu_h = 0.1$). (b) Effect of helix friction ($\mu_g = 0.7$). (c) Effect of link number ($\mu_g = 0.7$, $\mu_h = 0.1$).

where M_{robot} is the total mass of the robot, and $\overline{V}_{robot}$ is the average velocity of the robot head. The average mechanical output power of motor, $\bar{P}_{motor}$, can be obtained after multiplying T_{motor} by $\dot{\vartheta}$ and integrating the product.

Figure 8 shows the ADAMS simulation results for different friction coefficients and the link number n, when $\dot{\vartheta} = 2\pi$ rad/s. As illustrated in Fig. 8(a), COT is not monotonically decreasing with decreasing ground slipping, due to the increasing inertial effects caused by the velocity fluctuations. By keeping the value of μ_g constant and increasing the value of μ_h results in a higher COT. Hence a lower μ_h is preferred for SAW since significant energy dissipation would take place due to the helix friction, and $\overline{V}_{robot}$ is not sensitive to the helix friction, as observed in Fig. 8(b). During motion, some joints' constraint forces would press the links onto the helix and amplify the frictions. If the helix is smooth, SAW could have the same order of COT as snakes[25] (COT ≈ 1.15) or other robots driven by a single motor, such as 1STAR[26] and DASH,[27] whose COT are 0.73 and 1.42, respectively. Note that in this paper the idealized mechanical power is used for $\bar{P}_{motor}$. Taking the electric efficiency of the motor and other factors such as joint frictions into consideration would lead to a higher cost for the real SAW prototypes (COT ≈ 3.8 measured by Zarrouk[10]). The physical snake robots[28] are generally less efficient (COT > 10) when compared to SAW, caused by the common application of servo motors to realize the expected joint angles.

While only a few links contact the ground and propel the robot, more power is required to rotate the helix and lift other links. As a result, by decreasing the robot length (n and the length of the helix), the power consumption is decreased (see Fig. 8(c)). In the case that the robot is shorter than a wave length ($n = 7$), $\overline{V}_{robot}$ decreases obviously. Choosing the number of links that could form only one complete wave cycle would result in the most energy-efficient SAW, although a longer robot with more tips touching the ground would be more stable. The velocity of SAW predicted by Eq. (16) increases with the parameter A/L_{wave}, while qualitatively a higher wave peak with amplitude A would result in a higher mechanical transmission consumption to overcome gravity, and a narrow L_{wave} could cause a larger press as well as the friction between links and the helix.

https://doi.org/10.1017/S0263574719000389 Published online by Cambridge University Press

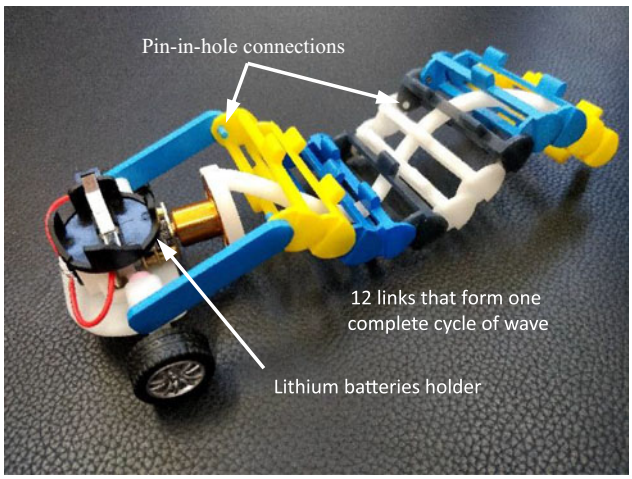


Fig. 9. Robot prototype of SAW.

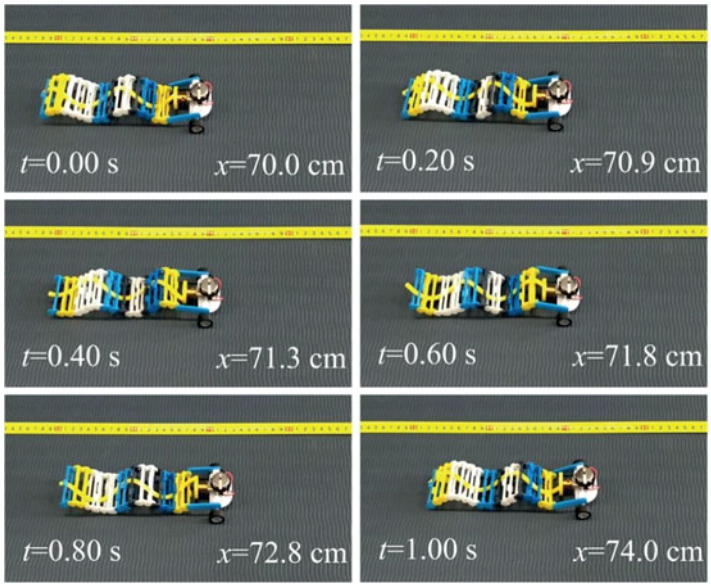


Fig. 10. Motion of SAW I on a carpet.

5. Prototypes and Experiments

Three robot prototypes were developed and tested on their kinematic performances. Figure 9 depicts the smallest robot prototype of SAW. The helix, links and the motor house were 3D printed and made of resin. A DC-geared motor was chosen, powered by lithium batteries of 6 V. Each link has through holes or pins at both ends; these pin-in-hole connections form the revolute joints without other connecting pieces.

SAW I has a length of 20 cm, and its total mass is 60 g. Two cycles of wave are formed by the helix and 17 links. The wave length is $L_{\text{wave}} = 8.0\,\text{cm}$, the wave amplitude is $A = 0.9\,\text{cm}$, and the height of each link is $2r = 1.8\,\text{cm}$. To reduce slip, SAW I was tested on a carpet, whose friction coefficient with the links is about 0.7. The motion of this prototype with $\dot{\vartheta} = 2\pi$ rad/s in one period is shown in Fig. 10. It can be observed that the robot moves with an unsteady velocity, and its average value is $\overline{V}_{\text{robotI}} \approx 4.0\,\text{cm/s}$, which is close to the analytical result $\overline{V}_{\text{lowestI}} = 4.78\,\text{cm/s}$. The smallest SAW II (Fig. 9) has a length of 16 cm and a mass of 50 g. This robot consists of a shorter helix and 12 links, comprising one complete sine wave. The robot prototypes with different lengths can be obtained similarly by removing some links and cutting the helix. The average velocity of SAW II on the carpet is $\overline{V}_{\text{robot}} \approx 3.5\,\text{cm/s}$, which is little less than that of SAW I. The comparison shows that the length parameter has little influence on the robot velocity, once at least one cycle of the wave is formed.

https://doi.org/10.1017/S0263574719000389 Published online by Cambridge University Press

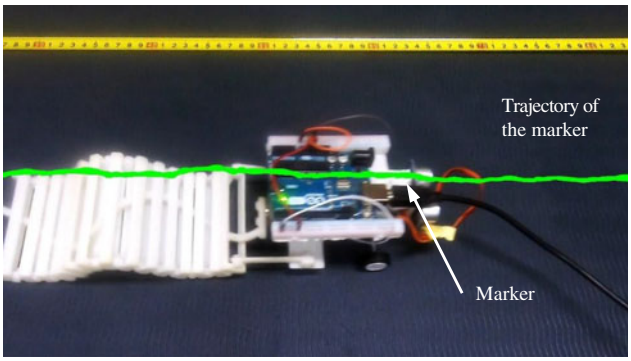


Fig. 11. Motion of SAW III and trajectory of the marker.

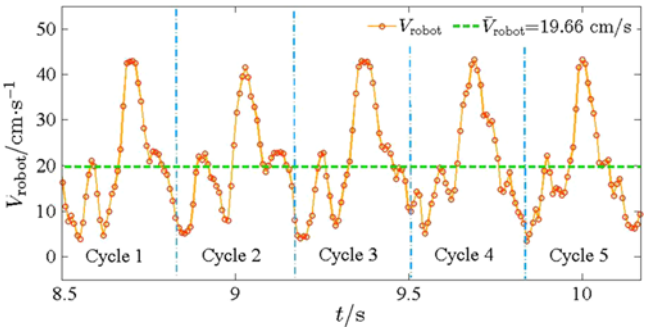


Fig. 12. Velocity of SAW III.

In order to acquire a velocity measurement of high accuracy, a faster SAW III ($A = 1.8$ cm, $L_{wave} = 12.0$ cm, see Fig. 11) is developed with a marker glued on the robot head, whose motion is recorded by GoPro camera (1080 p, 120 fps). The displacement of the marker in each video frame is determined to calculate the velocity by dividing the time interval, and a smoothing filter is adopted to eliminate the effect of the slight shaking of robot head shown in Fig. 11, which is caused by the impact contacts and assembly errors. Figure 12 shows the velocity of SAW III during five cycles; the curve contains a lower velocity peak in each cycle. This fluctuation trend is different from Fig. 6(b) due to the variation of the real motor rotation velocity affected by the torque load. The average experimental result $\overline{V}_{robotIII} = 19.66$ cm/s is close to the theoretical value $\overline{V}_{lowestIII} = 22.13$ cm/s, when the motor rotation velocity is kept as a constant $\dot{\vartheta} = 6\pi$ rad/s.

6. Conclusion

In this paper, the mechanism of a SAW-like robot is explored. The recursive relations for link position, velocity, and acceleration are derived, and the horizontal velocity of the link tip at wave trough is used to predict the robot velocity under no slipping conditions. The dynamic model of SAW is presented based on Kane's method. By comparing the simulation results of the robot velocity and the motor torque from the theoretical and ADAMS model, it is validated that the proposed models can effectively analyze the locomotion of this type of robot. Prototypes are developed, and their average velocities are in accord with the simulation results.

The performances of SAW are evaluated through simulations and experiments. The robot has a clever structure design, a small size, the convenience of manufacture, and some other advantages of traveling locomotion. An ordinary DC-geared motor is feasible to actuate SAW. However, it turns out that the velocity of SAW is not constant, and its power consumption is affected greatly by the friction between helix and links. From an energy-saving point of view, an optimal robot length is to form one wave cycle, and a rough link tip as well as a smooth helix is preferred.

For future work, structural optimization is demanded to improve the robot efficiency based on the mathematical model. A soft helix structure and micro-electro mechanical technics may contribute to the further development of SAW, which are also our interests.

https://doi.org/10.1017/S0263574719000389 Published online by Cambridge University Press

Acknowledgments
Support from the National Natural Science Foundation of China (Grant No. 11872223) towards this paper is gratefully appreciated.

References

1. J. Gray, "The mechanism of locomotion in snakes," *J. Exp. Biol.* **23**(23), 101–120 (1946).
2. S. G. Ma, "Analysis of Snake Movement Forms for Realization of Snake-like Robots," *Proceedings IEEE International Conference on Robotics and Automation*, Detroit, Michigan, USA (1999) pp. 3007–3013.
3. R. Ariizumi, M. Tanaka and F. Matsuno, "Analysis and heading control of continuum planar snake robot based on kinematics and a general solution thereof," *Adv. Rob.* **30**(5), 301–314 (2016).
4. M. Yim, K. Roufas, D. Duff, Y. Zhang, C. Eldershaw and S. Homans, "Modular reconfigurable robots in space applications," *Autonom. Rob.* **14**(2–3), 225–237 (2003).
5. L. Chen, S. G. Ma, Y. C. Wang, B. Li and D. P. Duan, "Design and modelling of a snake robot in traveling wave locomotion," *Mech. Mach. Theory* **42**(12), 1632–1642 (2007).
6. H. Kalani, A. Akbarzadeh and J. Safehian, "Traveling wave locomotion of snake robot along symmetrical and unsymmetrical body shapes," *Robotics* **26**(3), 1–7 (2011).
7. A. Rafsanjani, Y. R. Zhang, B. Y. Liu, S. M. Rubinstein and K. Bertoldi, "Kirigami skins make a simple soft actuator crawl," *Sci. Rob.* **3**(15), eaar7555 (2018).
8. Q. B. Pei, M. Rosenthal, S. Stanford, and H. Prahlad, "Multiple-degrees-of-freedom electroelastomer roll actuators," *Smart Mater. Struct.* **13**(5), 86–92 (2004).
9. M. Yim, D. Duff and K. Roufas, "PolyBot: A Modular Reconfigurable Robot," *Proceedings on IEEE International Conference on Robotics and Automation*, San Francisco, California, USA (2002) pp. 514–520.
10. D. Zarrouk, M. Mann, N. Degani, T. Yehuda, N. Jarbi and A. Hess, "Single actuator wave-like robot (SAW): Design, modeling, and experiments," *Bioinspiration Biomimetics* **11**(4), 046004 (2016).
11. A. Gao and A. H. Techet, "Design considerations for a robotic flying fish," *Oceans IEEE*, Waikoloa, Hawaii, USA (2011) pp. 1–8.
12. M. Saito, M. Fukaya and T. Iwasaki, "Serpentine locomotion with robotic snakes," *Control Syst. IEEE* **22**(1), 64–81 (2002).
13. S. G. Ma, N. Tadokoro, K. Inoue, and B. Li, "Influence of Inclining Angle of a Slope to Optimal Locomotion Curves of a Snake-like Robot," *IEEE International Conference on Robotics, Intelligent Systems and Signal Processing*, Changsha, China (2003) pp. 353–358.
14. P. Liljeback, K. Y. Pettersen, O. Stavdahl and J. T. Gravdahl, *Snake Robots: Modeling, Mechatronics, and Control* (Springer, Berlin, Germany, 2013).
15. E. Rezapour, K. Y. Pettersen, P. Liljebäck and G. T. Gravdahl, "Path following control of planar snake robots using virtual holonomic constraints: Theory and experiments," *Rob. Biomimetics* **1**(1), 3–19 (2014).
16. P. Prautsch and T. Mita, "Control and Analysis of the Gait of Snake Robots," *Proceedings of the IEEE International Conference on Control Applications*, Ohala Coast, Hawaii, USA (1999) pp. 502–507.
17. T. R. Kane and D. A. Levinson, "The use of Kane's dynamical equations in robotics," *Int. J. Rob. Res.* **2**(3), 3–20 (1983).
18. W. Nukulwuthiopas, T. Maneewan and S. Laowattana, "Dynamic Modeling of a One-wheel Robot by Using Kane's Method," *IEEE International Conference on Industrial Technology*, Bangkok, Thailand (2002) pp. 524–529.
19. C. Yang, Q. Huang and J. Han, "Decoupling control for spatial six-degree-of-freedom electro-hydraulic parallel robot," *Rob. Comput. Integr. Manuf.* **28**(1), 14–23 (2012).
20. J. E. Keat, "Comment on 'Relationship between Kane's equations and the Gibbs-Appell equations'," *J. Guidance Control Dyn.* **10**(6), 593–597 (2015).
21. T. R. Kane and D. A. Levinson, *Dynamics: Theory and Applications*, 1st ed., Series in Mechanical Engineering (McGraw-Hill, New York, 1985).
22. A. Meghdari, R. Karimi, H. N. Pishkenari, A. L. Gaskarimahalle and S. H. Mahboobi, "An effective approach for dynamic analysis of rovers," *Robotica* **23**(11), 771–780 (2005).
23. H. T. Nia, H. N. Pishkenari and A. Meghdari, "A recursive approach for the analysis of snake robots using Kane's equations," *Robotica* **24**(2), 251–256 (2006).
24. H. X. Wei, T. M. Wang and M. Liu, "Inverse dynamic modeling and analysis of a new caterpillar robotic mechanism by kane's method," *Robotica* **31**(3), 493–501 (2013).
25. M. Walton, B. C. Jayne and A. F. Bennett, "The energetic cost of limbless locomotion," *Science* **249**(4968), 524–527 (1990).
26. D. Zarrouk and R. S. Fearing, "Controlled in-plane locomotion of a hexapod using a single actuator," *IEEE Trans. Rob.* **31**(1), 157–167 (2015).
27. P. Birkmeyer, K. Peterson and R. S. Fearing, "DASH: A Dynamic 16g Hexapedal Robot," *IEEE/RSJ International Conference on Intelligent Robots & Systems, IEEE*, St. Louis, Missouri, USA (2009) pp. 2683–2689.
28. E. Kelasidi, P. Liljeback, K. Y. Pettersen and J. T. Gravdahl, "Experimental investigation of efficient locomotion of underwater snake robots for lateral undulation and eel-like motion patterns," *Rob. Biomimetics* **2**(1), 8 (2015).

https://doi.org/10.1017/S0263574719000389 Published online by Cambridge University Press

Appendix: Derivation of Eq. (13)

Taking the time derivative on Eq. (7) leads to:

$$x_1\dot{x}_1 + y_1\dot{y}_1 = 0 \tag{A1}$$

$$\dot{x}_1 = \dot{x}_{C1} + (L_{\text{link}} \cdot \sin\alpha_1)\dot{\alpha}_1/2 \tag{A2}$$

$$\dot{y}_1 = \tan\alpha_1 \cdot (\dot{x}_{C1} + \dot{\vartheta}/k) - (L_{\text{link}} \cdot \cos\alpha_1)\dot{\alpha}_1/2 \tag{A3}$$

$$\begin{aligned}\dot{\alpha}_1 &= \frac{-Ak\sin(kx_{C1}+\vartheta)}{1+[Ak\cos(kx_{C1}+\vartheta)]^2} \cdot (k\dot{x}_{C1} + \dot{\vartheta}) \\ &= -Ak^2 \cdot \sin(kx_{C1}+\vartheta)\cos^2\alpha_i \cdot (\dot{x}_{C1} + \dot{\vartheta}/k) \\ &= \beta_1 \cdot (\dot{x}_{C1} + \dot{\vartheta}/k)\end{aligned} \tag{A4}$$

where $\beta_1 = -k^2 \cdot \cos^2\alpha_1 \cdot y_{C1}$. Substitute $\dot{\alpha}_1$ from Eq. (A4) into Eqs. (A2) and (A3):

$$\dot{x}_1 = \dot{x}_{C1} + L_{\text{link}}\beta_1 \sin\alpha_1 \cdot (\dot{x}_{C1} + \dot{\vartheta}/k)/2 \tag{A5}$$

$$\dot{y}_1 = \big(\tan\alpha_1 - L_{\text{link}}\beta_1 \cdot \cos\alpha_1/2\big)(\dot{x}_{C1} + \dot{\vartheta}/k) \tag{A6}$$

Then Eq. (A1) becomes

$$\begin{aligned}&x_1\big[\dot{x}_{C1} + L_{\text{link}}\beta_1 \sin\alpha_1 \cdot (\dot{x}_{C1} + \dot{\vartheta}/k)/2\big] \\ &\quad + y_1\big(\tan\alpha_1 - L_{\text{link}}\beta_1 \cdot \cos\alpha_1/2\big)(\dot{x}_{C1} + \dot{\vartheta}/k) = 0\end{aligned} \tag{A7}$$

The goal is to express $\dot{x}_{C1}$ as a function of $\dot{\vartheta}$ and other variables, which have already been obtained after solving link positions, such as x_1, α_1, and β_1. Thus, Eq. (13) is given from Eq. (A7)

$$\dot{x}_{C1} = -\frac{\xi \cdot \dot{\vartheta}}{k(x_1 + \xi)}$$

where $\xi = y_1 \tan\alpha_1 + \beta_1 L_{\text{link}} \cdot (x_1 \sin\alpha_1 - y_1 \cos\alpha_1)/2$.

Equation (13) can also be derived under the condition that the 0th links rotate about a fixed axis in the frame U. The velocity of the first joint should be vertical to 0th links,that is,

$$[x_1, y_1, 0]^{\mathrm{T}} \cdot [\dot{x}_1, \dot{y}_1, 0]^{\mathrm{T}} = 0 \tag{A8}$$

which is equivalent to Eq. (A1). The motion of the first joint is a combination of link 1 on the wave and the rotating 0th links. Based on this principle, the position, velocity, and acceleration of the first link CM can be calculated and used as the start point of recursions to determine other links' motion.

https://doi.org/10.1017/S0263574719000389 Published online by Cambridge University Press